Metrology Requirements of State-of-the-Art Protection Schemes for DC Microgrids

Chunpeng Li*, Puran Rakhra*, Patrick Norman*, Graeme Burt*, Paul Clarkson†
*University of Strathclyde, Glasgow, UK
†National Physical Laboratory, London, UK

Keywords: DC microgrid; DC fault analysis; power system protection; smart grid.

Abstract

Environmental incentives to combat climate change are providing the motivation to improve the energy efficiency of power distribution systems and integrate state-of-the-art renewable technologies. Examples include wind/PV resources, energy storage systems and electric vehicles integrated via efficient power electronic converters (PEC). Subsequently, DC microgrids (MGs) and distribution systems are receiving considerable attention in the literature because they offer a simple, yet flexible, interface between these modern resources and consumers. However, many technical challenges relating to the design and standardization of DC protection devices still exist that must be overcome prior to widespread adoption. For example, many protection schemes tailored for DC MGs have been proposed but few of them have considered the metrology requirements for practical implementation. This paper will first review the key features of DC-side fault transients simulated on a DC MG model in MATLAB/Simulink, and analyse the disruptive impact on PEC components. Secondly, a review of newly published DC protection schemes is performed. These protection schemes are classified by their fundamental operating principles and mathematically-derived metrology requirements are given.

1 Introduction

Recent advancements in power electronic converter technologies have resulted in the development of high-efficiency AC-DC conversion, enabling high-voltage DC (HVDC) power transmission [1] and low-voltage DC (LVDC) distribution systems [2]. Whilst HVDC has already been widely installed in many countries, the commercial rollout of multi-terminal DC distribution systems still requires further research, development and standardisation before being extensively utilised.

DC microgrids offer many advantages including higher end-to-end energy efficiency and easier integration of modern energy resources [2] in comparison to conventional AC microgrids. Energy efficiency improvements are gained because such systems do not suffer from skin effect and fewer conversion stages are required [3]. Additionally, DC MGs provide a simpler platform for the integration of state-of-the-art renewable technologies through efficient power electronics [2], including wind/PV resources, energy storage systems and electric vehicles, etc.

To date, DC distribution networks have not been widely used in public power systems. Their applications are constrained to small-scale electricity networks such as telecommunications, aircraft, and marine power systems [3]. The main obstacles of commercial DC distribution networks have been expensive converters and the lack of direct consumers of DC power. However, recent trends show that costs of PECs are decreasing and user demand for DC power is increasing, raising the viability of near term future DC MGs [4].

One of the remaining challenges is the development of effective DC protection schemes that are designed for multi-terminal LVDC distribution networks [3]. The main difficulty results from the unconventional fault current response of a DC system, which creates two issues for protection. The first relates to the discharge of filter capacitors in response to a short circuit. This causes a rapidly increasing transient fault current peak which presents a damage risk to any electronic components in the fault path if not interrupted by fast acting DC protection. The other issue is that the DC fault current will not necessarily have zero crossing points for easier current interruption, requiring the use of large circuit breakers. Even though many researchers have made substantial efforts in developing theoretically effective DC MG protection strategies, few of them consider the metrology requirements for practical implementation.

This paper will study the fundamental characteristics of DC faults verified using a DC MG model, and derive the new metrology requirements of recently proposed LVDC protection schemes. Section 2 will review the theoretical derivation of DC-side fault transients, and analyse the disruptive impact of PECs on fault current transient behaviour. Section 3 will then classify and review the existing state-of-the-art protection schemes in terms of their fundamental operating principles. Finally, a mathematical analysis of the metrology requirements of each category of protection schemes is performed.

2 DC fault behaviour in DC microgrids

To design effective protection strategies for interconnected DC networks and assign measurement requirements for specific protection schemes, a review of DC-side short-circuit fault behaviour of converter-fed DC MGs is required. Taking a Voltage Source Converter (VSC) fed network as an example, this section will review the theoretical derivation of the DC-side short-circuit fault response. Subsequently, a case study using a DC MG model built in MATLAB/Simulink is conducted to analyse the disruptive impact of PECs on fault current transient behaviour.

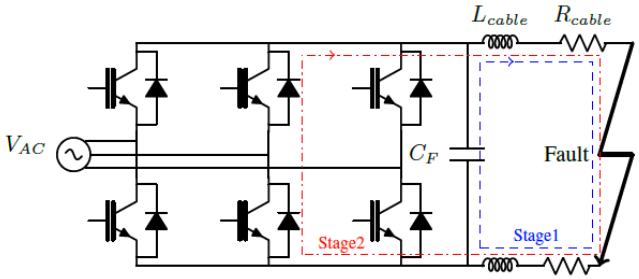

Fig. 1. Circulation stages of a VSC pole-to-pole fault.

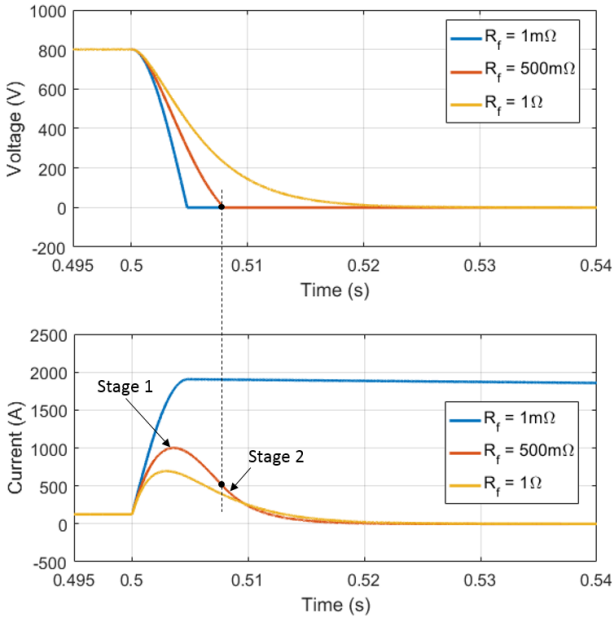

Fig. 2. Voltage/current profiles of a pole-to-pole fault (disabled converter infeed).

2.1 Review of DC short-circuit theory

Fig. 1 illustrates an equivalent model of a pole-to-pole short-circuit fault [4] whilst Fig. 2 shows the voltage and current responses to a range of fault resistances. The fault response can be divided into three stages as proposed in [5].

During Stage 1, a high-magnitude current transient caused by the discharge of the capacitors occurs, lasting from the fault initiation to the zero-voltage condition. This behaviour is evident in Fig. 2. The mathematical derivation of this current response can be obtained from the equation of an RLC circuit

$$\frac{d^2i(t)}{dt^2} + \frac{R}{L}\frac{di(t)}{dt} + \frac{1}{LC}\cdot i(t) = 0, \quad (1)$$

such that

$$i(t) \approx \frac{v_C(0)}{L\omega_d} e^{-\alpha t}\sin(\omega_d t), \quad (2)$$

where R, L, C are the equivalent resistance, inductance and capacitance of the fault path; $v_C(0)$ is the pre-fault voltage on the capacitor; α is the damping factor defined as $\alpha = R/2L$; ω_0 is the resonant radian frequency defined as $\omega_0 = 1/\sqrt{LC_F}$; ω_d is the damped resonant frequency defined as $\omega_d = \sqrt{\omega_0^2 - \alpha^2}$. The peak of the current profile occurs during this stage. Before this, the protection should operate in order to avoid exposure to excessive fault current magnitudes. However, this can be particularly challenging to achieve because the available time window of protection operation is very narrow. According to (2), for severely low resistance faults, the rate of change of current can be derived by

$$\frac{di(t)}{dt} \approx \frac{v_C(0)}{L}\cos(\omega_0 t), \quad (3)$$

where the peak point can be approximated as $(\frac{\pi}{2\omega_0}, \frac{V}{L\omega_0})$.

Stage 2 can be defined as the freewheeling stage, lasting from the zero-voltage condition to the steady-state current condition. For lower impedance faults, an underdamped current response is realized in which the fault current circulates through the antiparallel diodes within the converter, as illustrated in Fig. 1. This behaviour presents a significant risk of damage to components if the fault is not removed from the circuit by the protection devices prior to this stage [5].

Stage 3 is the grid feeding stage. After the steady-state current condition is reached, the primary side of the converter provides the fault current contribution through the antiparallel diodes of rectifier [5].

2.2 Case study: short-circuited behaviour of a multi-terminal DC microgrid

This subsection presents a case study to compare the theoretical fault response of a simplified RLC circuit, presented in Section 2.1, to the fault response of a short-circuited DC MG model.

In a multi-terminal DC MG, it can be assumed that the current infeed from a network-interfaced VSC is not disabled immediately following a fault. Furthermore, DC MGs are likely to integrate additional PECs involving more complex filter arrangements, such as LC circuits, with unknown fault response characteristics. To investigate the fault behaviour of such interconnected DC systems, a representative model of a DC MG was built within the MATLAB/Simulink environment. A diagram of this system is presented in Fig. 3.

In Fig. 3, the DC MG is connected to the AC utility with a 2-level bi-directional AC-DC VSC [4], regulating the link voltage to +/-375 V on the DC-side. The model of the photovoltaic (PV) system is based on the configuration presented in [6] and utilizes a boost converter to regulate the panel voltage at 54 V to achieve maximum power transfer. The battery array (10 × 12 V) is based on the dynamic model presented in [7], and uses a Dual Active Bridge (DAB) converter [8] to achieve bi-directional power transfer. The electronic load employs a buck converter [4], representing a typical constant voltage load requiring high-quality power. Each of the components connects to the bus through a pair of cables with different distances as shown in Fig. 3.

For each branch of the DC MG, the simulated fault current in response to a 1 mΩ fault on the main distribution busbar is recorded and is compared to the theoretical waveform obtained using equation (2). Taking the AC grid interface branch as an example, the comparison illustrated in Fig. 4 indicates that the fault current behaviour prior to the occurrence of the first peak shows good alignment.

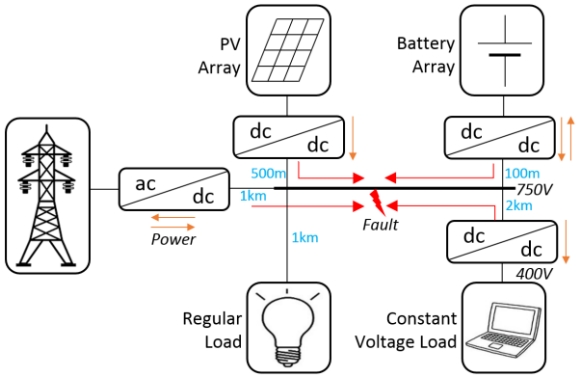

Fig. 3. Diagram of a DC microgrid.

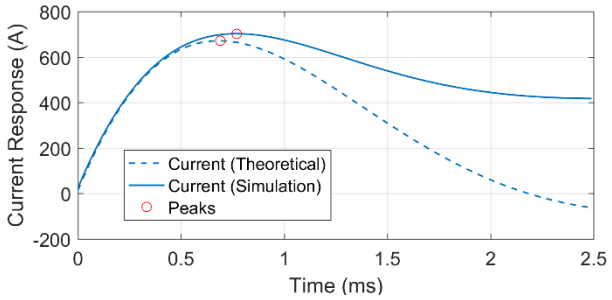

Fig. 4. Comparison between the theoretical fault response and simulation results of DC MG fault response at grid feeder.

Branch	Theoretical Calc.	Simulation	Errors
AC Grid	(0.69ms, 672A)	(0.77ms, 703A)	(10%, 4%)
Regular Load	-	(0, 18A)	-
PV Array	(0.52ms, 1122A)	(0.52ms, 1133A)	(0, 1%)
Battery Array	(0.26ms, 3134A)	(0.25ms, 3039A)	(4%, 3%)
Const. Volt. Load	(0.91ms, 369A)	(0.91ms, 360A)	(0, 3%)

Table 1. Comparison of theoretical and simulated peaks.

Further analysis presented in Table 1 summarizes the comparison of simulation and theoretical results of peak magnitude and peak time for the fault current measured at each branch. The results obtained show that the errors of all theoretical predictions are less than 10% from that of the simulated responses.

The close similarity between theoretical calculation and simulation result indicates that the capacitor discharge dominates the fault current transient. Accordingly, the following can be deduced:

a. For low impedance short circuit faults, where there is a sufficient decoupling between the responses of individual branches of the DC MG, the transient fault current can be reliably approximated by the presented analysis of the nearest RLC circuit.

b. The converter contribution of fault current in response to a low-impedance fault does not impact on the magnitude of the first current peak associated with the capacitor discharge. Typically the time constant associated with this source of fault current is significantly greater than that of a dc side filter capacitor discharge and as such can often be neglected. Note that for high bandwidth power sources typically employed for power quality regulation and/or higher impedance fault conditions, this assumption of negligible converter source contribution towards the first current peak may not be valid.

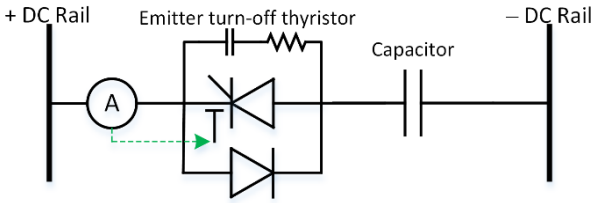

Fig. 5. ETO-based capacitive discharge circuit breaker [9].

3 Study of state-of-the-art protection schemes

Recently, many researchers have proposed a number of tailor-made protection schemes for DC MGs. In terms of their fundamental principles, this section will review and classify state-of-the-art protection schemes, and investigate the corresponding challenges of measurement in practical applications for each classification.

3.1 Type I: Instantaneous overcurrent protection

Before the concept of DC MGs was proposed, there already existed many small-scale DC electricity applications such as the wiring and electrical equipment for vehicles, requiring protection solutions. These were mainly realised with instantaneous overcurrent protection devices, such as fuses and electromagnetic switches [3]. Such devices require no separate components for measurement, relay processing, and current breaking, however, the drawbacks are also obvious. On one hand, these devices are difficult to coordinate for backup protection, and cannot realise large-scale network protection. On the other hand, these devices are frequently employed effectively in battery-based DC networks, but the protection speed is not fast enough that it can be applied in VSC-based network protection, as described in Section 2.1.

After the invention of solid-state switches, such as Thyristor ETO, MOSFET, IGBT, etc., ultra-fast protection was achievable [4]. The work presented by Mahajan and Baran in [9] represents one of the most comprehensive efforts to design a protection scheme for a VSC interfaced network. For the issue of capacitive discharge, the authors propose the use of instantaneous overcurrent protection for solid-state power electronic switches to interrupt capacitive discharge currents. This is achieved through the connection of an ETO device in series with the capacitive element, as shown in Fig. 5. The operating principle is based on the current sensing of the ETO which is compared to a threshold. When the capacitor current crosses this threshold, a hard turnoff is initiated which limits any further increase and interrupts the current in $3-7\ \mu s$.

However, in practical applications, it is difficult for the measurement sensors to reliably detect the transient fault current. Based on the description in the previous section, the current sensor must possess the following two features:

a. Wide measurement bandwidth. To ensure the measured current is sufficiently accurate to the real fault current, the bandwidth of measurement must be higher than the fault current bandwidth. The highest fault current bandwidth appears in the condition of a short-circuit fault ($R \approx 0$), that is $\omega_0/2\pi$, typically 200Hz.

b. High sampling frequency. As the numerical comparison is conducted by a digital processor, the A/D converter must utilise a high sampling frequency for taking fast protection actions. The sampling time setting depends on the peak time and the number of sample captures required before the time of current peak. Defining the desired number of samples as N, the minimum sampling rate, f_S, can be derived, such that

$$f_S = \frac{N}{0.25T_0} = \frac{N}{0.5\pi\sqrt{LC}}. \quad (4)$$

For example, assuming the natural frequency of a fault is 250 Hz ($T_{peak} = 1\ ms$), and the desired number of samples before the peak current is 1000, the minimum sampling rate is 1 MHz. Whilst this approach is suitably fast acting to solve the issue of capacitive discharge for the network described within this paper, the approach is far less effective when higher levels of protection selectivity are desired. That is, ensuring that only the local protection operates for a fault at a particular location in the network. To solve this issue, differential and non-unit protection schemes are proposed.

3.2 Type II: Protection schemes based on differential measurement

A method of high-speed differential protection for smart DC distribution systems is proposed by Fletcher in [10]. It utilizes the natural characteristics of DC differential current measurements to significantly reduce fault detection times, and hence meet requirements for DC converter protection (2ms). This method measures the boundary currents of a protected zone and utilizes a communication link to compare the currents based on Kirchhoff's current law, such that

$$\Delta i = i_1(t) + i_2(t). \quad (5)$$

Fig. 6 illustrates the schematic diagram of the internal and external faults. When the sum of currents is greater than a threshold setting, it indicates that a fault exists within the protected zone. When the sum is a low value, it indicates that the network is healthy or there exists an external fault for which the local protection should keep stable. This method offers ultrafast protection with effective selectivity. However, this method requires a large number of SSCBs and communication links with the ensuing high installation costs. Additionally, it does not inherently provide backup protection in the event of device trip-failure.

To overcome the issue of no backup protection, Monadi reinforced this method with a zonal design [11], as shown in Fig. 7. This scheme conducts a current comparison not only between the nearest relays but also between further relays in the event of a failure of low-level zone protection. However, in order to realise effective backup protection, the protection devices have to complete the progress of fault detection, attempting operation in Zone 1, detecting the failure of operation, attempting operation in Zone 2, etc. in the very narrow time window. Therefore, it is challenging to implement this protection scheme in practice.

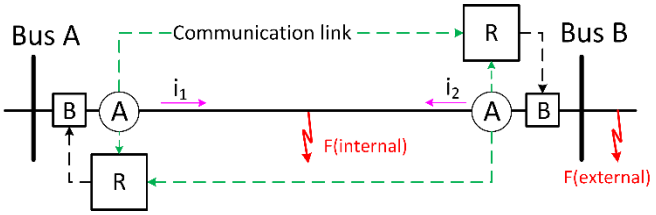

Fig. 6. Illustration of internal and external faults.

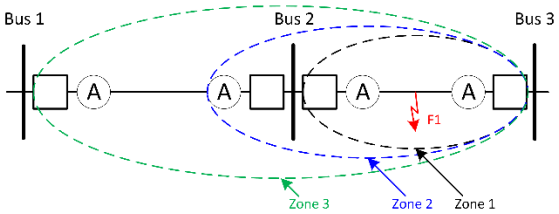

Fig. 7. Differential scheme with backup protection [11].

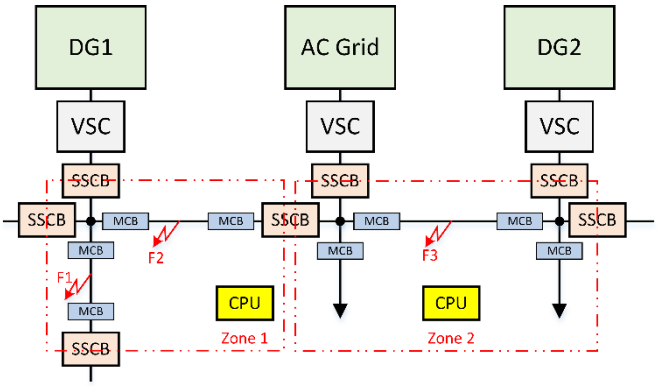

Fig. 8. Centralised protection configuration [12].

As for the issue of requiring a large number of SSCBs, Monadi also proposed a centralised protection strategy, as shown in Fig. 8. This scheme only utilizes SSCBs at the boundaries of large zones and terminals of VSCs, while applying only common mechanical isolators on the distribution lines [12]. As a fault occurs, the SSCB operates rapidly to isolate the faulted zone, while the isolators locate the faulted line based on differential protection. Since the zone has been de-energized with the SSCBs, the mechanical isolators can easily isolate the faulted line within a relaxed time-window. After the fault is cleared, the SSCBs will reclose to re-energize the healthy part of the network zone. This scheme enables the probability of realising secure protection schemes for large-scale DC microgrids, but with a dependence on reliable, high-bandwidth data transmission.

In order to minimise the amount of data transmitted through communication links, Emhemed and Burt proposed a directional-based protection scheme for LVDC distribution networks [13], as shown in Fig. 9. This scheme employs a centralised protection device to gather and process data on current directions rather than values. When the currents on the two ends of a line are detected as flowing in opposite directions, it indicates that a short-circuit fault has occurred within the zone. The centralized digital relay unit can offer effective backup protection, but also poses a risk, as it is a single point of failure of the protection system. Additionally, since the protection is only based on current direction, it may be ineffective for detecting high-impedance faults.

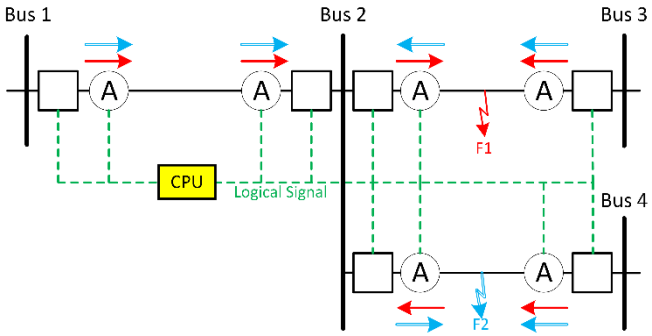

Fig. 9. Illustration of directional protection operation [13].

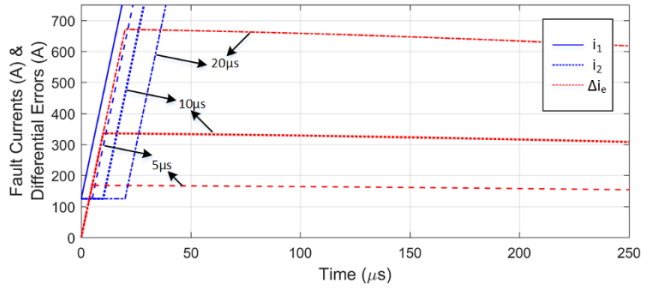

Fig. 10. Illustration of the time synchronisation issue [10].

V_C	L	$I_{Threshold}$ $setting$
$10^3\ V$	$10 \times 10^{-6}\ H$	$10^2\ A$

Table 2. Example of network parameters.

The four protection schemes analysed in this subsection commonly use differential protection based on communication links. The major challenge of Type II protection schemes is time synchronised measurement, because even a very small synchronisation error may result in protection mal-operation. For example, Fletcher demonstrated in [10] that the small synchronization errors can cause significant differential errors, as shown in Fig. 10. According to (3), if the rate of current (di/dt) before the peak is estimated as V_C/L, the maximum error caused by the imperfect synchronisation can be derived, whereby

$$\Delta i_e = \frac{V_C}{L}\Delta T_e. \tag{6}$$

Δi_e must be lower than the threshold setting to ensure the protection is stable for external faults. However, assuming the order of the practical network parameters in Table 2 are applied, the requirement of time synchronization measurement may be as narrow as $\Delta T_e < 1\mu s$. This is a comparative level to an inherent physical delay over a distance of 300m.

3.3 Type III: Protection schemes based on rate of change of measurement

Since Type II protection schemes have implementation challenges associated with time synchronised measurements, another type of protection is proposed which utilizes the rate of change of a local measurand. A patent utilising initial rate of change of current (di/dt) was granted by Fletcher in [14] for an LVDC protection application. According to Kirchhoff's voltage law,

$$\frac{\mathrm{di(t)}}{\mathrm{dt}} = \frac{v_{C_F}(t) - i_L(t)R}{L}. \tag{7}$$

At the initiation of a short-circuit fault, that is $t = 0^+$, the term $i_L(t)R$ is approximately zero and can therefore be neglected. Accordingly, the cable inductance, which represents the distance from the capacitor to the fault location, can be derived by the pre-fault voltage and the initial di/dt measurement, where

$$L \cong \frac{v_{C_F}(0^+)}{\mathrm{di}(0^+)/\mathrm{dt}}. \tag{8}$$

Since this method utilises the initial characteristics of the fault transient, it can theoretically estimate fault distance within the first two samples after fault initiation, enabling the operation of protection at lower current levels. Additionally, this protection method can offer effective backup protection by discriminating the fault locations. However, the drawbacks include that this protection principle does not allow any shunt capacitors to be connected which are commonly employed in PECs and electronic loads, causing the protection to be ineffective in the event of a failure to accurately detect the initial di/dt value.

In order to overcome the risk of missing the initial di/dt measurement, Feng has reinforced the scheme with an optimised approach [15]. Measuring voltage, current and di/dt every 20-100 μs, the simultaneous equations can be solved to determine R and L, where by

$$\begin{bmatrix} L \\ R \end{bmatrix} = (A^T A)^{-1} A^T B. \tag{9}$$

$$A = \begin{bmatrix} \frac{di}{dt}(0) & i(0) \\ \frac{di}{dt}(1) & i(1) \\ \vdots & \vdots \\ \frac{di}{dt}(N) & i(N) \end{bmatrix} \qquad B = \begin{bmatrix} v(0) \\ v(1) \\ \vdots \\ v(N) \end{bmatrix}$$

This method not only overcomes the risk of missing the initial fault point, but also is capable of distinguishing low-resistance and high-resistance faults. However, as a downside to this method is that it takes a long time to detect a fault. Other methods based on dv/dt and d^2i/dt^2 have also been proposed in the literature but have not been proven in practice.

The metrology requirements of Type III protection schemes are particularly challenging because derivative computation is extremely sensitive to very small noise. So, signal conditioning is required for optimising the derivative computation [16]. According to [16], the appropriate sampling time should first be selected. Extremely short sampling time will magnify the noise by numerical derivative computation, while excessively long sampling times will result in attenuated di/dt results and time delays. A digital low-pass filter may be needed to constrain the high-frequency noise before the numerical derivative computation.

3.4. Summary

Table 3 summarizes the advantages and drawbacks of the state-of-the-art schemes described in this paper, and the challenges of measurement of each.

Type	Scheme Name	Advantage	Disadvantage	Measurement Challenge
Type I: Overcurrent	Fuse/EM switch	Compact	Slow Difficult in realising selectivity	n/a
	ETO-SSCB	High-speed	No selectivity	High bandwidth High sampling rate (>1MHz)
Type II: Differential protection	Differential	High-speed High selectivity	Provides no backup protection Require large number of SSCBs Need communication links	Require accurate time-synchronised measurement (synchronisation error<5μs).
	Differential with backup	Provides backup protection	Require large number of SSCBs Need communication links	
	Centralised	Less usage of SSCBs Provides backup protection	Need communication links	
	Directional	Less data transmission Provides backup protection	Not sensitive to high R faults Risk of using centralised relay	
Type III: Rate of change protection	Initial di/dt	High-speed Selectivity No need for communication	Risk of missing initial sample Shunt capacitor not allowed Not reliable with signal sample	Derivative computation is extremely sensitive to the noise, requiring appropriate computational step-times and low-pass filters.
	Multiple di/dt	Higher reliability Both R & L are detectable	Shunt capacitor not allowed	

Table 3. Summary of protection schemes.

4 Conclusion

This paper has categorised state-of-the-art protection schemes for DC MGs and derived new metrology requirements for each, with a focus on the measurement challenges associated with practical implementation. It was found that instantaneous overcurrent protection requires wide-bandwidth measurement sensors and ultrafast sampling rates to avoid missing the initial fault current peak. Differential protection schemes require very accurate time-synchronised measurements with minimal time synchronisation error that may cause protection mal-operation in the event of external faults. Particularly, in a compact DC network where a high di/dt exists, this requirement may be too difficult to achieve practically. Non-unit protection schemes based on the rate-of-change of local measurands to avoid the use of communication links were also presented. However, numerical derivative computation is very sensitive to noise so signal conditioning should be applied, including selecting appropriate computational time-steps and effective low-pass filters.

The authors believe that the findings in this paper place an emphasis on redefining the focus of the dc protection research community. Whilst current efforts focus on addressing the limitations in state-of-the-art solid-state and mechanical technologies (e.g., fault withstand in PECs, current interruption in SSCBs, selectivity/speed of breakers), this paper has shown that this approach may result in unrealisable solutions because the metrology requirements have not been sufficiently considered. The findings presented provide a strong argument to consider metrology capabilities/limitations as part of the technology solution in order to realise impactful and game-changing research. In the future, the authors plan to demonstrate the value of this new perspective by delivering near-term realisable, novel DC MG protection solutions shaped by practical measurement constraints.

Acknowledgements

The authors would like to thank National Physical Laboratory, UK for providing financial support to conduct this research.

References

[1] W. Long and S. Nilsson, “HVDC transmission: yesterday and today,” *IEEE Power Energy Mag.*, vol. 5, no. 2, pp. 22–31, 2007.
[2] P. Brian, “DC, come home: DC microgrids and the birth of the ‘enernet,’” *IEEE Power Energy Mag.*, vol. 10, no. 6, pp. 60–69, 2012.
[3] S. Fletcher, “Protection of physically compact multi-terminal DC power systems,” Ph.D. thesis, *Strathclyde Univ.*, Glasgow, UK, 2013.
[4] N. Mohan, *et al.*, “Power electronics: converters, applications and designs,” 3rd ed., Minnesota: *John Wiley & Sons, Inc.*, 2003.
[5] J. Yang *et al.*, “Short-circuit and ground fault analyses and location in VSC-based DC network cables,” *IEEE Trans. Ind. Electron.*, vol. 59, no. 10, pp. 3827–3837, 2012.
[6] M. M. Rajan Singaravel, *et al.*, “MPPT with single DC-DC converter and inverter for grid connected hybrid wind-driven PMSG-PV system,” *IEEE Trans. Ind. Electron.*, vol. 62, no. 8, pp. 4849–4857, 2015.
[7] O. Tremblay and L. A. Dessaint, “Experimental validation of a battery dynamic model for EV applications,” *World Electro. Veh. J.*, vol. 3, no. 1, pp. 289–298, 2009.
[8] B. Zhao *et al.*, “Overview of dual-active-bridge isolated bidirectional DC-DC converter for high-frequency-link power-conversion system,” *IEEE Trans. Power Electron.*, vol. 29, no. 8, pp. 4091–4106, 2014.
[9] M. E. Baran and N. R. Mahajan, “Overcurrent protection on voltage-source-converter-based multi-terminal dc distribution systems,” *IEEE Transactions on Power Delivery*, vol. 22, no. 1, pp. 406-412, Jan, 2007.
[10] S. Fletcher, P. Norman, K. Fong, S. Galloway, and G. Burt, “High-speed differential protection for smart DC distribution system,” *IEEE Trans. Smart Grid*, vol. 5, no. 5, pp. 2610-2617, 2014.
[11] M. Monadi, *et al.*, “A communication-assisted protection scheme for direct-current distribution networks,” *Energy J.*, vol. 109, no. c, pp. 578-591, 2016.
[12] M. Monadi, *et al.*, “Centralized protection strategy for medium voltage dc microgrid,” IEEE Trans. Power Delivery, vol. 32, no. 1, 2016.
[13] A. Emhemed, and G. Burt, “An advanced protection scheme for enabling an LVDC last mile distribution network,” *IEEE Trans. on Smart Grid*, vol. 5, no. 5, pp. 2602-2608, 2014.
[14] S. Fletcher, P. Norman, and S. Galloway, “Protection system for an electrical power network,” *U.S. Patent 8 842 401 B2*, Sep. 23, 2014.
[15] X. Feng, *et al.*, “A novel fault location method and algorithm for DC distribution protection,” *IEEE Trans. Ind. App.*, vol. 53, no. 3, pp. 1834-1840, 2017.
[16] C. Li, *et al.*, “Practical computation of di/dt for high-speed protection of DC microgrids,” *IEEE 2nd International Conf. on DC Microgrid*, pp. 153-159, 2017.